SCIENCE CHINA
Technological Sciences

• Article •

December 2014 Vol.57 No.12: 2487–2499
doi: 10.1007/s11431-014-5723-x

Semi-analytical solution for fully developed forced convection in metal-foam filled tube with uniform wall temperature

ZHANG JiaJie, QU ZhiGuo*, XU HuiJin & TAO WenQuan

MOE Key Laboratory of Thermo-Fluid Science and Engineering, School of Energy and Power Engineering, Xi'an Jiaotong University, Xi'an 710049, China

Received August 26, 2014; accepted November 11, 2014

Fully developed flow and heat transfer in metal-foam filled tube with uniform wall temperature (UWT) is semi-analytically investigated based on the Brinkman–Darcy model and the two-equation model, in which the inertia term, axial conduction, and thermal dispersion are ignored. A two-dimensional numerical simulation that adopts the full governing equations is also conducted to analyze the effects of neglected terms on flow and thermal transport performance by comparing with the semi-analytical solution. The effects of the relevant parameters and thermal boundary conditions including UWT and uniform heat flux (UHF) on the heat transfer characteristics are discussed based on the semi-analytical solution. The results show that the inertia term has a significant effect on the prediction of pressure drop, but has a relatively mild effect on Nusselt number. The axial conduction has significant effect on the Nusselt number at lower Reynolds number, and the effects of thermal dispersion can be neglected when the thermal conductivity ratio between fluid and solid is remarkably smaller for air/metal foam as example ($k_f/k_s<3\times10^{-3}$). The predicted Nusselt number of the semi-analytical solution is about 8% to 15% lower than that of the numerical solution with full model in the range of $4\times10^{-5}<k_f/k_s<3\times10^{-3}$. Moreover, the temperature profile of solid is more sensitive to pore density and porosity than that of fluid under UWT condition. The Nusselt number under UWT is about 7% to 25% lower than that under UHF, and the difference is mainly determined by interfacial convection rather than solid conduction.

metal foams, semi-analytical, uniform wall temperature, numerical simulation, heat transfer

Citation: Zhang J J, Qu Z G, Xu H J, et al. Semi-analytical solution for fully developed forced convection in metal-foam filled tube with uniform wall temperature. Sci China Tech Sci, 2014, 57: 2487–2499, doi: 10.1007/s11431-014-5723-x

Nomenclature

a_{sf}	specific surface area, [m^{-1}];
Bi_e	dimensionless quantity, $h_{sf}a_{sf}R^2/k_{se}$;
c	specific heat capacity [J kg^{-1} K^{-1}];
C_I	inertia coefficient;
C_D	thermal dispersion constant;
d_f	fiber diameter of metal foam [m];
d_p	pore size of metal foam [m];
Da	Darcy number;
h	heat transfer coefficient [W m^{-2} K^{-1}];
k	thermal conductivity [W m^{-1} K^{-1}];
k_d	thermal dispersion coefficient [W m^{-1} K^{-1}];
K	permeability [m^2];
L	axial length of tube [m];
Nu	Nusselt number, $2h_xR/k_f$;
p	pressure [Pa];
P	dimensionless pressure;
Pr	Prandtl number;
$q_{w,x}$	local heat flux at the wall [W m^{-2}];
r	radial coordinate [m];
R	tube radius [m];

*Corresponding author (email: zgqu@mail.xjtu.edu.cn)

Re Reynolds number, $\rho u(2R)/\mu$;
Re_K permeability Reynolds number, $\rho u\sqrt{K}/\mu$;
T temperature [K];
$T_{f,b}$ bulk-mean temperature of fluid [K];
u axial velocity [m s^{-1}];
u_m mean axial velocity [m s^{-1}];
U dimensionless velocity;
v radial velocity [m s^{-1}];
x axial coordinate [m].

Greek symbols

ε porosity
η dimensionless radial coordinate, r/R;
μ dynamic viscosity [kg m^{-1} s^{-1}];
θ dimensionless temperature, $(T-T_w)/(T_{f,b}-T_w)$;
ρ density [kg m^{-3}];
ω pore density of metal foam, pores per inch (ppi=$0.0254/d_p$).

Subscripts

b bulk;
e effective;
f fluid;
in inlet;
s solid;
w wall.

1 Introduction

The energy shortage and environmental pollution have become the significant issues with the development of the industry and economy. Therefore, many advanced materials and technologies have been developed to improve the efficiency of energy utilization [1–3]. Metal foams, as a kind of novel porous medium with high porosity and high thermal conductivity, may exhibit excellent thermal performance when used in compact exchangers and heat sinks due to its high surface-area density and strong flow-mixing capability. This attractive advantage gives rise to extensive investigations on flow and heat transport phenomena in metal-foam filled structures in recent years.

In principle, metal foams with open cells belong to porous media in which the medium has a distinct but continuous and rigid solid phase, and a fluid phase. The most common theoretical models for describing flow transfer in porous media are the Darcy and the non-Darcy models. For the flow with low Reynolds number in the porous medium, such as ground-water hydrology, petroleum reservoir, and geothermal operations, the Darcy model is generally adopted to investigate the flow transport features [4]. However, the Darcy model has significant deviations for flow prediction with high Reynolds number due to neglecting viscous force of impermeable boundary and inertia force; the effects of viscous force and inertia force in the porous media were discussed in detail by Vafai and Tien [5]. Considering these non-Darcy effects, the Brinkman-Darcy model and the Brinkman-Forchheimer-Darcy model were proposed, the former includes the boundary effect, whereas the latter includes both the boundary and the inertia effects. Hooman [6] analytically studied the fully developed forced convection through a porous medium filled with parallel plates based on the Brinkman–Forchheimer-Darcy model by applying the asymptotic expansion technique. Zhao et al. [7] then solved the same flow model for flow characteristics in a channel filled with porous media by utilizing the homotopy analysis method. Dukhan [8] applied the Brinkman–Darcy model to analytically study the flow characteristics in a cylindrical porous tube, and conducted a related verification experiment using aluminum foam. The predicted friction factor from the analytical solution agreed well with the experimental data for the foam, with 20 pores per inch (ppi) in the Darcy regime. In present study, the Brinkman–Darcy model is used as the momentum equation to describe the flow characteristics in metal-foam filled tube.

While for heat transfer in porous media, the one-equation or the two-equation models can be adopted. The fluid and solid phases are assumed in local thermal equilibrium in the one-equation model so that the fluid-saturated porous medium can be treated as a continuum. Hooman and Merrikh [9] used the one-equation model combining with the Brinkman-Darcy model, to obtain a Fourier series type of solution for thermally fully developed convection in a hyperporous-medium filled rectangular duct with constant heat flux on the walls. Also, based on the one-equation model and the non-Darcy model, Chikh et al. [10] analytically investigated forced convection in porous-medium partially filled pipe, in which the inner is exposed to constant heat flux and the outer is thermally insulated. Zhu et al. [11] carried out a numerical study on heat transfer inside rotating porous disk subjected to uniform heat flux. However, the one-equation model was found to be inaccurate when the difference between thermal conductivity of fluid and porous solid is significant, just as the case of metal foam involved in present study. While the two-equation model can be applied because it treats the fluid and solid separately, and considers the local temperature difference between the fluid and solid. Yang et al. [12] applied the one-equation and two-equation models to analyze comparatively the forced convection in a tube with wall covered with porous medium layer under constant heat flux boundary condition. The results showed that the two-equation model was more accurate than the one-equation model when the temperature difference between the solid and fluid was obvious. Calmidi and Mahajan [13] used the non-Darcy model and the

two-equation model to conduct a numerical and experimental study on forced convection in aluminum-foam filled tube with uniform heat flux boundary condition, and the excellent agreement between the experimental and the numerical results confirmed the effectiveness of the two-equation model. In addition, the literatures [14–21] applied the non-Darcy model and the two-equation model to investigate forced convection heat transfer in different structures filled with metal foam under constant heat flux condition. Therefore in this study, the two-equation model is employed as the energy equation to analyze the heat transfer in metal-foam filled tube.

The above mentioned studies about convection heat transfer in porous medium adopted the uniform heat flux (UHF) as the thermal boundary condition. For the condition of uniform wall temperature (UWT), Kamiuto and Saitoh [22] theoretically studied the fully developed convection in a cylindrical packed bed, Hooman et al. [23] and Nield et al. [24] analyzed thermally developing convection in porous medium filled with rectangular ducts and parallel channels, respectively. However, these studies on porous medium under UWT condition all used the one-equation model as energy equation, this model will be inappropriate for the case of metal foam based on the above reviews. Nield et al. [25] employed the two-equation model to investigate the thermally developing convection in porous media filled parallel-plate channel with UWT condition for the case of low porosity (ε=0.5) and high fluid-solid thermal conductivity ratio ($k_f/k_s \geqslant 0.1$), but due to the difficulties in solving convergence, the case of high porosity ($\varepsilon \geqslant 0.85$) and low thermal conductivity ratio ($k_f/k_s<0.01$) was not involved, which just are the feature of metal foams.

As reviewed, the previous studies about convection heat transfer in porous medium mostly adopt the UHF thermal boundary condition. Few literatures consider the UWT condition, particularly for metal foam with two-equation model. This may be due to the fact that accurately solving the energy equation under the UWT condition is hard, and also few experimental data are available because of the difficulty in the implementation of UWT thermal environment. However, in practical applications there are also many constant wall temperature cases such as the steam condensate heating, wall cooling in catalytic reaction, and plate-fin heat exchanger with UWT condition [26] and so on. Therefore, considering the potential applications of metal foams in above cases, the related study about metal foams with UWT condition is necessary and significant. In the current study, a semi-analytical investigation on fully developed forced convection in a metal-foam filled tube with UWT is conducted by applying the Brinkman–Darcy model and the two-equation model. A two-dimensional numerical simulation based on the full momentum and energy models is also performed to analyze the effects of the inertia term, axial conduction, and thermal dispersion, which are ignored in the semi-analytical study. In addition, the effects of relevant parameters on the heat transfer characteristics are discussed based on the semi-analytical solution. The boundary condition of UHF and UWT are compared for the temperature profile and Nusselt number.

2 Physical and mathematical model

2.1 Physical description

The geometric configuration for the forced convection through a tube filled with metal foams is shown in Figure 1. The metal foams are filled in a circular tube with a diameter of $2R$ and a length of L. The wall temperature was kept uniform and constant as the value of T_w. The fluid flows through the tube and exchanges heat with the tube wall through the metal foams. The steady and incompressible flow of fluid with constant physical properties is assumed while the natural convection and thermal radiation are both negligible. The metal foams filled in the tube are homogeneous and isotropic, and with constant physical properties.

2.2 Governing equation

The full momentum equations and energy equations based on the non–Darcy model and the two-equation model are presented as follows:

$$\frac{\partial u}{\partial x}+\frac{1}{r}\frac{\partial (rv)}{\partial r}=0, \tag{1}$$

$$\frac{\rho_f}{\varepsilon^2}\left[\frac{\partial (uu)}{\partial x}+\frac{1}{r}\frac{\partial (vru)}{\partial r}\right]=-\frac{\partial p}{\partial x}+\frac{\mu_f}{\varepsilon}\left[\frac{\partial^2 u}{\partial x^2}+\frac{1}{r}\frac{\partial}{\partial r}\left(\frac{\partial u}{\partial r}\right)\right] -\frac{\mu_f}{K}u-\frac{\rho_f C_1}{\sqrt{K}}|\boldsymbol{u}|u, \tag{2}$$

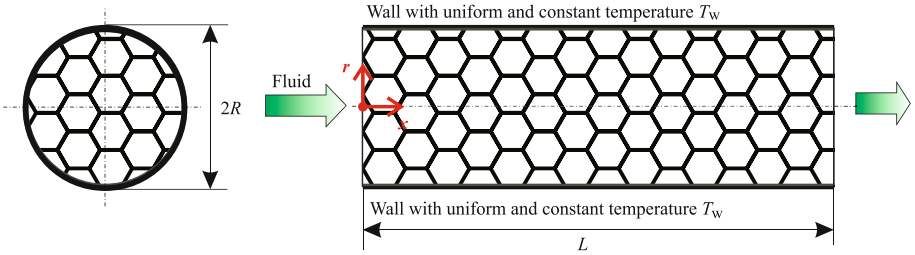

Figure 1 (Color online) Geometric configuration of the metal-foam filled tube.

$$\frac{\rho_{\mathrm{f}}}{\varepsilon^2}\left[\frac{\partial(uv)}{\partial x}+\frac{1}{r}\frac{\partial(rvv)}{\partial r}\right]=-\frac{\partial p}{\partial r}+\frac{\mu_{\mathrm{f}}}{\varepsilon}\left[\frac{\partial^2 v}{\partial x^2}+\frac{1}{r}\frac{\partial}{\partial r}\left(\frac{\partial v}{\partial r}\right)\right]-\frac{\mu_{\mathrm{f}}}{K}v-\frac{\rho_{\mathrm{f}}C_{\mathrm{I}}}{\sqrt{K}}|\boldsymbol{u}|v, \tag{3}$$

$$0=k_{\mathrm{se}}\left[\frac{\partial^2 T_{\mathrm{s}}}{\partial x^2}+\frac{1}{r}\frac{\partial}{\partial r}\left(\frac{\partial T_{\mathrm{s}}}{\partial r}\right)\right]-h_{\mathrm{sf}}a_{\mathrm{sf}}\left(T_{\mathrm{s}}-T_{\mathrm{f}}\right), \tag{4}$$

$$\rho_{\mathrm{f}}c_{\mathrm{f}}\left[\frac{\partial(uT_{\mathrm{f}})}{\partial x}+\frac{1}{r}\frac{\partial(vrT_{\mathrm{f}})}{\partial r}\right]=\frac{\partial}{\partial x}\left(\left(k_{\mathrm{fe}}+k_{\mathrm{d}}\right)\frac{\partial T_{\mathrm{f}}}{\partial x}\right)+\frac{1}{r}\frac{\partial}{\partial r}\left(\left(k_{\mathrm{fe}}+k_{\mathrm{d}}\right)\frac{\partial T_{\mathrm{f}}}{\partial r}\right)+h_{\mathrm{sf}}a_{\mathrm{sf}}\left(T_{\mathrm{s}}-T_{\mathrm{f}}\right), \tag{5}$$

where ε, K, C_{I} are the porosity, permeability, and inertia coefficients of the metal foams, respectively; a_{sf} and h_{sf} are the solid–fluid interfacial surface area density and the interfacial heat transfer coefficient, respectively; k_{se} and k_{fe} are the effective thermal conductivities of the solid and fluid, and k_{d} is the thermal dispersion coefficient.

The present study focuses on forced convection heat transfer with fully developed condition in a metal-foam filled tube. For the definition of fully developed flow, the radial velocity component is negligible and the axial velocity does not change along the axial direction, thence eq. (6) can be presented as follows [27]:

$$\frac{\partial u}{\partial x}=0,\quad v=0,\quad \frac{\mathrm{d}p}{\mathrm{d}x}=\text{constant}. \tag{6}$$

For the fully developed heat transfer, the heat transfer coefficient keeps constant and the first derivative of dimensionless temperatures for fluid and solid across the duct is zero, thence eqs. (7) and (8) hold as follows [27]:

$$\frac{\partial}{\partial x}\left(\frac{T_{\mathrm{f}}-T_{\mathrm{w}}}{T_{\mathrm{f,b}}-T_{\mathrm{w}}}\right)=0,\quad \frac{\partial}{\partial x}\left(\frac{T_{\mathrm{s}}-T_{\mathrm{w}}}{T_{\mathrm{f,b}}-T_{\mathrm{w}}}\right)=0, \tag{7}$$

$$h_x=\text{constant}. \tag{8}$$

Eq. (7) can be rewritten as follows:

$$\frac{\partial T_{\mathrm{f}}}{\partial x}=\frac{\mathrm{d}T_{\mathrm{w}}}{\mathrm{d}x}+\left(\frac{T_{\mathrm{f}}-T_{\mathrm{w}}}{T_{\mathrm{f,b}}-T_{\mathrm{w}}}\right)\frac{\mathrm{d}T_{\mathrm{f,b}}}{\mathrm{d}x}-\left(\frac{T_{\mathrm{f}}-T_{\mathrm{w}}}{T_{\mathrm{f,b}}-T_{\mathrm{w}}}\right)\frac{\mathrm{d}T_{\mathrm{w}}}{\mathrm{d}x}, \tag{9a}$$

$$\frac{\partial T_{\mathrm{s}}}{\partial x}=\frac{\mathrm{d}T_{\mathrm{w}}}{\mathrm{d}x}+\left(\frac{T_{\mathrm{s}}-T_{\mathrm{w}}}{T_{\mathrm{f,b}}-T_{\mathrm{w}}}\right)\frac{\mathrm{d}T_{\mathrm{f,b}}}{\mathrm{d}x}-\left(\frac{T_{\mathrm{s}}-T_{\mathrm{w}}}{T_{\mathrm{f,b}}-T_{\mathrm{w}}}\right)\frac{\mathrm{d}T_{\mathrm{w}}}{\mathrm{d}x}. \tag{9b}$$

For the wall condition with uniform heat flux (UHF), eq. (10a) holds.

$$\frac{\mathrm{d}T_{\mathrm{f,b}}}{\mathrm{d}x}=\frac{\mathrm{d}T_{\mathrm{w}}}{\mathrm{d}x}=\text{constant}. \tag{10a}$$

By substituting eq. (10a) into eqs. (9a) and (9b), eq. (10b) can be obtained.

$$\frac{\partial T_{\mathrm{f}}}{\partial x}=\frac{\partial T_{\mathrm{s}}}{\partial x}=\frac{\mathrm{d}T_{\mathrm{w}}}{\mathrm{d}x}=\text{constant}. \tag{10b}$$

Therefore, the axial conduction is exactly zero for the UHF condition as shown in eq. (10c)

$$\frac{\partial^2 T_{\mathrm{f}}}{\partial x^2}=\frac{\partial^2 T_{\mathrm{s}}}{\partial x^2}=0. \tag{10c}$$

For the present uniform wall temperature (UWT), eq. (11a) holds. Therefore, eqs. (9a) and (9b) can be rewritten as eq. (11b) in the following.

$$\frac{\mathrm{d}T_{\mathrm{w}}}{\mathrm{d}x}=0, \tag{11a}$$

$$\frac{\partial T_{\mathrm{f}}}{\partial x}=\left(\frac{T_{\mathrm{f}}-T_{\mathrm{w}}}{T_{\mathrm{f,b}}-T_{\mathrm{w}}}\right)\frac{\mathrm{d}T_{\mathrm{f,b}}}{\mathrm{d}x},\quad \frac{\partial T_{\mathrm{s}}}{\partial x}=\left(\frac{T_{\mathrm{s}}-T_{\mathrm{w}}}{T_{\mathrm{f,b}}-T_{\mathrm{w}}}\right)\frac{\mathrm{d}T_{\mathrm{f,b}}}{\mathrm{d}x}. \tag{11b}$$

Eq. (11b) indicates that the axial conduction is not zero for the UWT condition. Applying the law of energy conservation to a differential control volume of the tube, eq. (11c) can be obtained as follows:

$$\frac{\mathrm{d}T_{\mathrm{f,b}}}{\mathrm{d}x}=\frac{2h_x\left(T_{\mathrm{w}}-T_{\mathrm{f,b}}\right)}{\rho_{\mathrm{f}}c_{\mathrm{f}}u_{\mathrm{m}}R}. \tag{11c}$$

By substituting eqs. (6), (11b) and (11c) into eqs. (1) to (5), the governing equations for fully development convection in metal-foam filled tube under UWT can be obtained in eqs (12)–(14):

$$0=-\frac{\mathrm{d}p}{\mathrm{d}x}+\frac{\mu_{\mathrm{f}}}{\varepsilon}\left[\frac{\partial^2 u}{\partial x^2}+\frac{1}{r}\frac{\partial}{\partial r}\left(\frac{\partial u}{\partial r}\right)\right]-\frac{\mu_{\mathrm{f}}}{K}u-\frac{\rho_{\mathrm{f}}C_{\mathrm{I}}}{\sqrt{K}}|\boldsymbol{u}|u, \tag{12}$$

$$0=k_{\mathrm{se}}\left[\frac{\partial^2 T_{\mathrm{s}}}{\partial x^2}+\frac{1}{r}\frac{\partial}{\partial r}\left(\frac{\partial T_{\mathrm{s}}}{\partial r}\right)\right]-h_{\mathrm{sf}}a_{\mathrm{sf}}\left(T_{\mathrm{s}}-T_{\mathrm{f}}\right), \tag{13}$$

$$-\frac{u}{u_{\mathrm{m}}}\frac{2h_x}{R}\left(T_{\mathrm{f}}-T_{\mathrm{w}}\right)=\frac{\partial}{\partial x}\left[\left(k_{\mathrm{fe}}+k_{\mathrm{d}}\right)\frac{\partial T_{\mathrm{f}}}{\partial x}\right]+\frac{1}{r}\frac{\partial}{\partial r}\left[\left(k_{\mathrm{fe}}+k_{\mathrm{d}}\right)\frac{\partial T_{\mathrm{f}}}{\partial r}\right]+h_{\mathrm{sf}}a_{\mathrm{sf}}\left(T_{\mathrm{s}}-T_{\mathrm{f}}\right). \tag{14}$$

The corresponding boundary conditions are shown as follows:

$$r=R,\quad u=0,\ T_{\mathrm{s}}=T_{\mathrm{f}}=T_{\mathrm{w}}, \tag{15}$$

$$r=0,\quad \frac{\partial u}{\partial r}=\frac{\partial T_{\mathrm{f}}}{\partial r}=\frac{\partial T_{\mathrm{s}}}{\partial r}=0. \tag{16}$$

There are three typical nonlinear terms as follows: Inertia term of $-\frac{\rho_{\mathrm{f}}C_{\mathrm{I}}}{\sqrt{K}}|\boldsymbol{u}|u$ in eq. (12), axial conduction terms of

$k_{se}\dfrac{\partial^2 T_s}{\partial x^2}$ in eq. (13) and $\dfrac{\partial}{\partial x}\left[\left(k_{fe}+k_d\right)\dfrac{\partial T_f}{\partial x}\right]$ in eq. (14), and thermal dispersion terms of $\dfrac{\partial}{\partial x}\left[k_d\dfrac{\partial T_f}{\partial x}\right]$ and $\dfrac{1}{r}\dfrac{\partial}{\partial r}\left[k_d\dfrac{\partial T_f}{\partial r}\right]$ in eq. (14). Notably, eqs. (12)–(16) can be solved by numerical approach, but they are difficult to solve by analytical approach due to the existence of above three nonlinear terms. However, these nonlinear terms can be neglected for some typical conditions in practice. The inertia term has a limited effect on flow and heat transfer for the low permeability or low velocity cases as indicated in Vafai and Tien [5]. The axial conduction terms play little role when the heat convection is dominant where strong flow-mixing capability occurs in the metal-foam. In addition, the enhancing effects of thermal dispersion terms are extremely low for the porous medium with high thermal conductivity, such as the case of metal-foam [14]. Therefore, these nonlinear terms are usually removed when solving the analytical solution of forced convection in metal-foam [14–17]. Based on these, the three nonlinear terms are neglected in present semi-analytical study to facilitate the implementation of analytical approach. The effects of three neglected terms can be discussed by comparing with the late numerical solution with the complete model.

2.3 Normalization

After neglecting the inertial term, axial conduction term and thermal dispersion terms in eqs. (12)–(14), the equations and boundary conditions can be normalized by introducing the following dimensionless quantities:

$$\begin{aligned} &Da=\frac{K}{R^2},\ \eta=\frac{r}{R},\ U=\frac{u}{u_m},\ P=\frac{K}{\mu_f u_m}\frac{\mathrm{d}p}{\mathrm{d}x},\\ &\tau=\sqrt{\frac{\varepsilon}{Da}},\ \theta_f=\frac{T_f-T_w}{T_{f,b}-T_w},\ \theta_s=\frac{T_s-T_w}{T_{f,b}-T_w},\\ &Nu=\frac{h_x(2R)}{k_f},\ Bi_e=\frac{h_{sf}a_{sf}R^2}{k_{se}},\ \Gamma=\frac{k_{fe}}{k_{se}},\ \Psi=\frac{k_f}{k_{fe}}. \end{aligned} \tag{17}$$

The obtained dimensionless equations and boundary conditions are then presented as follows:

$$U+P=\frac{1}{\tau^2}\left(\frac{\partial^2 U}{\partial\eta^2}+\frac{1}{\eta}\frac{\partial U}{\partial\eta}\right), \tag{18}$$

$$0=\frac{\partial^2\theta_s}{\partial\eta^2}+\frac{1}{\eta}\frac{\partial\theta_s}{\partial\eta}-Bi_e\left(\theta_s-\theta_f\right), \tag{19}$$

$$-\Psi UNu\theta_f=\frac{\partial^2\theta_f}{\partial\eta^2}+\frac{1}{\eta}\frac{\partial\theta_f}{\partial\eta}+\frac{Bi_e}{\Gamma}\left(\theta_s-\theta_f\right), \tag{20}$$

$$\eta=1,\quad U=\theta_s=\theta_f=0, \tag{21}$$

$$\eta=0,\quad \frac{\partial U}{\partial\eta}=\frac{\partial\theta_f}{\partial\eta}=\frac{\partial\theta_s}{\partial\eta}=0. \tag{22}$$

3 The semi-analytical solution procedure

3.1 The momentum equation

The momentum equation, eq. (18), is a modified Bessel equation of zero order with a non-zero right-hand side, which can be solved as presented in the Appendix. Thus, the exact solution of velocity profile and pressure drop can be obtained as follows:

$$U=P\left[\frac{I_0(\tau\eta)}{I_0(\tau)}-1\right], \tag{23}$$

$$P=\frac{I_0(\tau)}{2I_1(\tau)/\tau-I_0(\tau)}, \tag{24}$$

where $I_0(\xi)$ and $I_1(\xi)$ are the first-type modified Bessel functions of zero order and first order and can be found in the Appendix.

3.2 The energy equations

After obtaining the exact velocity solution, the coefficients in eqs. (19) and (20) are known, except for Nu, which is related to temperature and is deduced in the following equations. The heat transfer on the tube wall occurs through the solid and the fluid phases [13], and then, the local heat flux on the tube wall can be presented in eq. (25).

$$q_{w,x}=h_x\left(T_{f,b}-T_w\right)=-\left(k_{se}\frac{\partial T_s}{\partial r}+k_{fe}\frac{\partial T_f}{\partial r}\right)\Bigg|_{r=R}. \tag{25}$$

Eq. (25) may be rewritten in the dimensionless form as eq. (26):

$$h_x=-\frac{k_{se}}{R}\left(\frac{\partial\theta_s}{\partial\eta}+\Gamma\frac{\partial\theta_f}{\partial\eta}\right)\Bigg|_{\eta=1}. \tag{26}$$

Substituting eq. (26) into the definition formula of Nu from eq. (17), the local Nusselt number can be expressed in eq. (27):

$$Nu=\frac{h_x(2R)}{k_f}=-\frac{2}{\Gamma\Psi}\left(\frac{\partial\theta_s}{\partial\eta}+\Gamma\frac{\partial\theta_f}{\partial\eta}\right)\Bigg|_{\eta=1}. \tag{27}$$

However, given that Nu depends on the dependent variables θ_f and θ_s, eqs. (19) and (20) can not be solved precisely. Consequently, an iteration approach is employed to solve the solid and fluid temperature profiles, and the Nu can be selected as the iterative parameter. Eq. (27) is not an appropriate iterative formula for the iteration convergence because it depends on the temperature gradient of

the tube wall. Adding eqs. (19) to (20) leads to the following equation:

$$-\Gamma\Psi NuU\theta_{\mathrm{f}}\eta=\frac{\partial}{\partial\eta}\left[\eta\frac{\partial(\theta_{\mathrm{s}}+\Gamma\theta_{\mathrm{f}})}{\partial\eta}\right]. \tag{28}$$

Integrating both sides of eq. (28) along the radial direction and introducing eq. (27) would yield the following equation:

$$-\Gamma\Psi Nu\int_0^1(U\theta_{\mathrm{f}}\eta)\mathrm{d}\eta=\left(\frac{\partial\theta_{\mathrm{s}}}{\partial\eta}+\Gamma\frac{\partial\theta_{\mathrm{f}}}{\partial\eta}\right)\Bigg|_{\eta=1}=-\frac{\Gamma\Psi}{2}Nu. \tag{29}$$

Hence, a recommended iterative formula of Nu with the integral form can be obtained by rewriting eqs. (29) to (30).

$$Nu^{n+1}=Nu^n\Big/2\int_0^1(U\eta\theta_{\mathrm{f}}^n)\mathrm{d}\eta. \tag{30}$$

For the implementation of iterative calculation, eqs. (19) and (20) are discretized with a central difference scheme, with a uniform grid system for the dimensionless radius η, and the grid number is selected as 381 after a grid independence checking among 351, 381 and 411. The velocity solutions of eqs. (23) and (24) are substituted into the discrete equations of eqs. (19) and (20). The iteration flow chart for the energy equation is shown in Figure 2. The iteration process includes the internal iteration and external iteration. The internal iteration is performed to obtain the improved $\theta_{\mathrm{f}}^n, \theta_{\mathrm{s}}^n$ by employing the coupling three diagonal matrix algorithm [28], and the convergence criterion is shown in eq. (31). The external iteration is conducted to obtain the final convergence values of Nu^n, while satisfying the condition in eq. (32)

$$\frac{\theta_{\mathrm{s}}^{n+1}-\theta_{\mathrm{s}}^n}{\theta_{\mathrm{s}}^n}\leqslant10^{-4},\ \frac{\theta_{\mathrm{f}}^{n+1}-\theta_{\mathrm{f}}^n}{\theta_{\mathrm{f}}^n}\leqslant10^{-4}, \tag{31}$$

$$\frac{Nu^{n+1}-Nu^n}{Nu^n}\leqslant10^{-7}. \tag{32}$$

4 Two-dimensional numerical simulation

4.1 Numerical model

A two-dimensional numerical model is established on the whole domain of the tube (Figure 1) including the entrance region and the fully developed region. The numerical method may well deal with the nonlinear terms in governing equations by employing the appropriate discretization approach [29–31]. Therefore, the complete conjugate heat transfer model including inertia terms, axial conduction terms, and thermal dispersion terms are employed for the numerical solution with the governing equations of eqs. (1)–(5). The corresponding boundary conditions are shown in eqs. (33) to (36), where the inlet velocity and temperature are fixed for fluid phase, and adiabatic condition is selected for solid phase at the tube entrance, whereas the local–unidirectional assumption for flow and heat transfer are adopted for both fluid and solid phases at the tube outlet when the Peclet number is high enough. The uniform and constant temperature is imposed at the tube wall, as well as the no-slip condition for flow, and the symmetric boundary is used for the axis of the tube.

$$x=0:\ u=u_{\mathrm{in}},\ v=0,\ T_{\mathrm{f}}=T_{\mathrm{in}},\ \frac{\partial T_{\mathrm{s}}}{\partial x}=0, \tag{33}$$

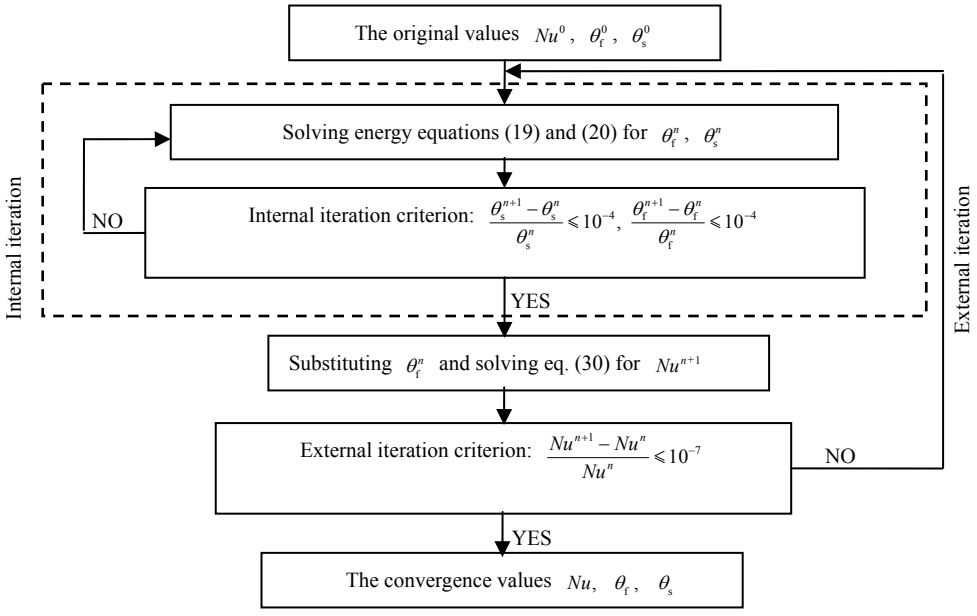

Figure 2 Iteration flow chart.

$$x = L: \quad \frac{\partial u}{\partial x} = \frac{\partial v}{\partial x} = \frac{\partial T_f}{\partial x} = \frac{\partial T_s}{\partial x} = 0, \tag{34}$$

$$r = 0: v = 0, \quad \frac{\partial u}{\partial r} = \frac{\partial T_f}{\partial r} = \frac{\partial T_s}{\partial r} = 0, \tag{35}$$

$$r = R: \quad u = v = 0, \quad T_f = T_s = T_w. \tag{36}$$

4.2 Numerical approach

The numerical calculation is performed based on the CLEAR algorithm [32], and the governing equations are discretized using the central difference scheme for diffusion terms and the stability-guaranteed second-order difference (SGSD) scheme for the convective terms [33]. The ratio of tube length and radius, *L*/*R*, is fixed as 40 to ensure the full development of flow and heat transfer in the porous medium. Non-uniform grid based on hyperbolic tangent function is adopted for the *r* direction, whereas uniform grid is arranged for the *x* direction. The grid independence is checked, and the final grid number is selected as 152(*x*)×32(*r*). The convergence criterion is that the relative variation of pressure drop and the average Nusselt number between two successive iterations are less than 10^{-5} and 10^{-7}, respectively.

5 Results and discussion

5.1 Comparative feasibility for the semi-analytical and numerical solutions

The correctness of semi-analytical approach is first verified with the numerical results with neglecting the inertial, axial conduction and thermal dispersion terms. The effects of these three terms can be further investigated with compassion results between the semi-analytical results and numerical results with the complete model. To present the semi-analytical and two-dimensional numerical solutions, the air is selected as work fluid through the metal-foam filled tubes. The pertinent parameters of metallic foam, such as K, C_I, a_{sf}, h_{sf}, k_{se}, k_{fe}, k_d, are calculated by adopting the semi-empirical correlations shown in Attached Table. The thermal physical properties of air are selected as the values at 20°C, and the flow of Reynolds number for each case is no more than 2000 to fulfill the laminar flow pattern in porous media (correspondingly, Re_K<100 [34]). The air inlet temperature and the tube wall temperature are respectively fixed at 293.15 and 273.15 K in the two-dimensional numerical simulation.

Figure 3 displays the dimensionless fluid and solid temperature distributions in the whole tube, these results are transformed from dimensional solution of the two-dimensional numerical simulation by using eq. (17). The numbers in figure means the dimensionless temperature value and thence the dimensionless wall temperature (defined in eq. (17)) is constant as 0. The intensive temperature variations for the fluid and solid in the entrance region of the tube are detected. The temperature variation of the fluid and solid gradually weakens away from the entrance region, and finally, the dimensionless fluid and solid temperature become constant values when $x > 0.6L$ ($L = 40R$), indicating that the flow and heat transfer have accessed the fully developed region. This result also implies that the thermal entrance length of the porous-media filled tube ($x/R \approx 24$) is much shorter than that of smooth tube ($x/R \approx 0.068RePr$=100 [35]). Meanwhile, since the given numerical results include the thermal entrance region and fully developed region, the semi-analytical solution can be verified by the numerical results extracted in the fully developed region (x=0.8L) by substituting the dimensional numerical results into the dimensionless definition formulas of eq. (17).

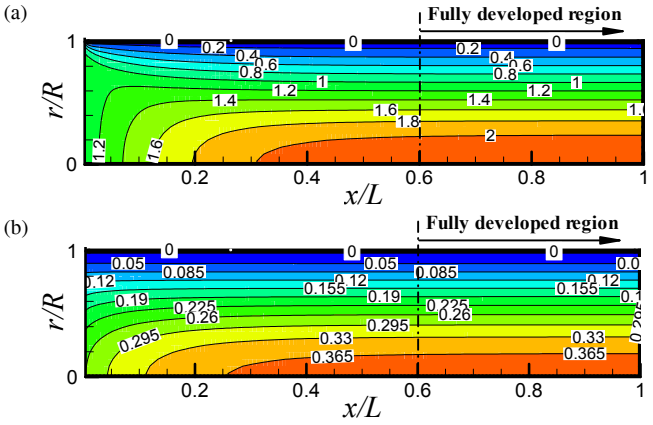

Figure 3 (Color online) Dimensionless temperature fields in the whole tube filled with porous foam from the numerical solution (ω=10 ppi, ε=0.90, k_f/k_s=10^{-4}, Re=2000, R=0.005 m). (a) Dimensionless fluid temperature θ_f; (b) dimensionless solid temperature θ_s.

5.2 Fluid flow characteristics

5.2.1 Velocity distribution

Figure 4 shows the dimensionless velocity profile comparison for the analytical solution and numerical solutions with inertia term and without inertia term. The corresponding velocity profile for the smooth tube is also presented as reference. The analytical solution and numerical solution without the inertia term are in good agreement. However, the inertia term has an obvious effect on velocity distribution when considered. The velocity gradient with inertia effect near the tube wall is enlarged, and the fluid velocity in the tube center area is lowered compared to that without inertia term. This result is attributed to the inertia force introducing a damping for flow in porous medium. In addition, the foam-filled tube has thinner hydrodynamic boundary layer and more uniform velocity distribution than the smooth tube because the existence of foam ligaments makes the velocity profile uniform.

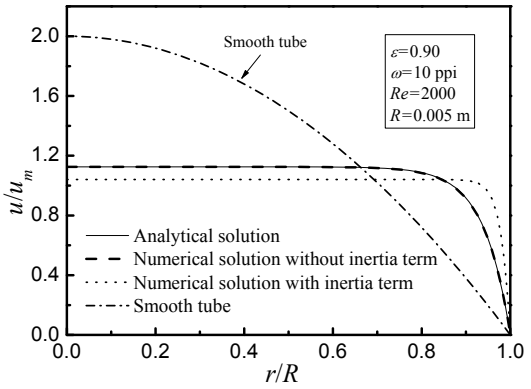

Figure 4 Dimensionless velocity profile of the tube radial section.

5.2.2 Pressure drop

Figure 5 displays the pressure drop variation with Reynolds number for different solving models. The pressure drop in the foam-filled tube increases with increasing Reynolds number. The pressure drop of the analytical solution agrees well with that of the numerical solution without inertia effect. Meanwhile, when the inertia term is considered in the numerical model, the pressure drop under a fixed Reynolds number becomes amplified, and the effect becomes more significant for the case with higher Reynolds number or higher pore density. This result implies that the inertial term has a dominant role on the pressure drop for the high Reynolds number flow in porous foam.

5.3 Temperature profile

5.3.1 Effects of interia term, axial conduction and thermal dispersion

Figures 6(a) and (b) depict the comparison of temperature profiles of the fluid and solid in metal-foam filled tube under different solving models. In Figure 6(a), the axial conduction, inertial term, and thermal dispersion are artificially removed in the numerical model to realize the identical assumption with the present semi-analytical solution. The

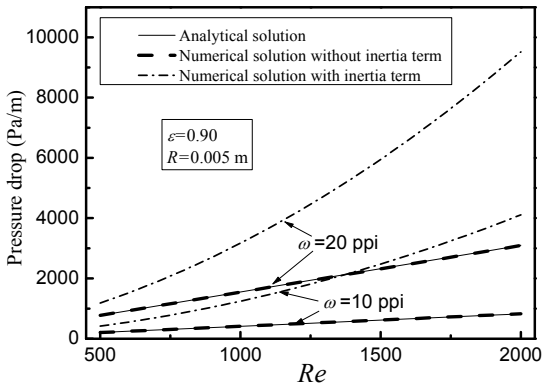

Figure 5 Comparison of the variation of pressure drop with Reynolds number for different solving models.

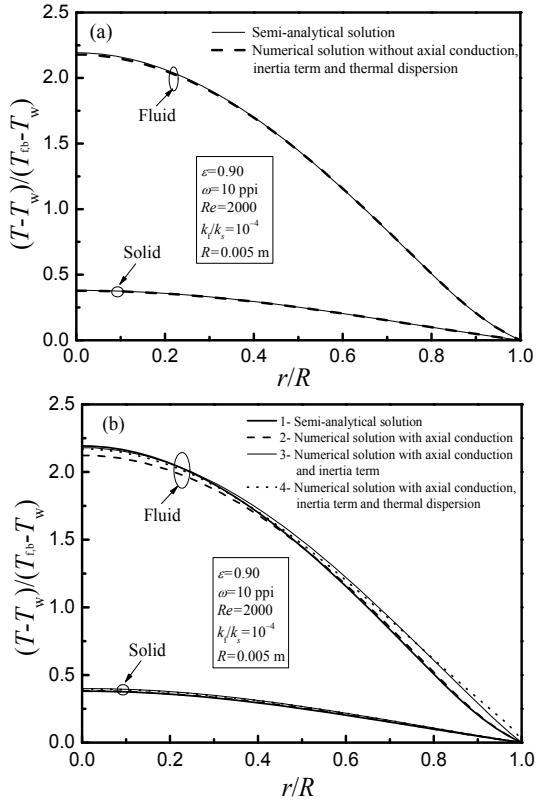

Figure 6 Comparison of temperature profiles for different solving models. (a) Semi-analytical solution and numerical solution with identical model; (b) semi-analytical solution and numerical solutions with different models.

temperature profiles of the semi-analytical and the numerical solutions are in good agreement with identical assumptions, thereby the feasibility of semi-analytical solution is verified. Meanwhile, in Figure 6(b), the axial conduction, inertia term, and thermal dispersion are successively added in the numerical model for cases 2, 3, and 4. By comparing case 1 vs. case 2, case 2 vs. case 3, and case 3 vs. case 4, the effects of axial conduction, inertia term, and thermal dispersion on the temperature profiles can be identified. It's seen that the three terms have the relatively clearer impacts on the temperature profile of fluid than that of solid. The dimensionless fluid temperature is reduced in the tube center region ($r/R<0.4$) by adding the axial conduction (case 1 vs. case 2). The addition of inertia term (case 2 vs. case 3) increases the fluid temperature gradient near the tube wall. Moreover, the effect of thermal dispersion is hardly discernible from case 3 vs. case 4. This result shows that, when the thermal conductivity of fluid is much less than that of the solid ($k_f/k_s=10^{-4}$), the dominant role of heat transfer in the porous foam is through the solid conduction and interfacial convection, and the fluid thermal dispersion has little effect on heat transfer performance, as also indicated in [13].

5.3.2 Effects of pore density and porosity

Figures 7(a) and (b) show the effects of pore density and porosity on the fluid and the solid temperature profiles, respectively. Porosity and pore density are two important morphology parameters that determine the porous morphology of metal foam; porosity is a fraction of the volume of voids over the total volume of foam, and pore density is defined as the pores per inch of the foam ($\omega=0.0254/d_{\mathrm{p}}$).

In Figure 7(a), when the pore density varies from 10 to 20 ppi under fixed porosity of 0.90, the temperature difference between the solid matrix and the fluid notably decreases. This decrease is ascribed to the reduction in the foam ligament diameter and the improvement of associated specific surface area with increasing pore density at fixed porosity (as indicated in Attached Table), thereby leading to stronger interfacial convection and lower solid–fluid temperature difference. In Figure 7(b), when the porosity varied from 0.85 to 0.95 under fixed pore density of 10 ppi, the solid dimensionless temperature increases, this also means that the temperature difference between solid matrix and wall increases. This result is due to that the effective thermal conductivity reduces with increasing porosity under the other parameters fixed. Thus, the heat conduction thermal resistance inside the foam matrix increases, accompanied with increased temperature difference between the solid and the wall. Generally as shown in Figure 7(a) and (b), the solid temperature profile is much more sensitive to the variation of foam morphology parameters than that of the fluid. The phenomenon is different from the case of UHF in reference [14], in which the fluid temperature profile is much more sensitive to morphology parameters than that of the solid. This difference between the UHF and UWT can be explained from the conclusion obtained by Wang et al. [36,37] that the heat flux normal to the wall is transported mostly by diffusion under UWT condition, whereas by convection under UHF condition. This result implies that the solid temperature and fluid temperature profiles are more susceptible to the morphology parameters of porous media for UWT and UHF conditions, respectively.

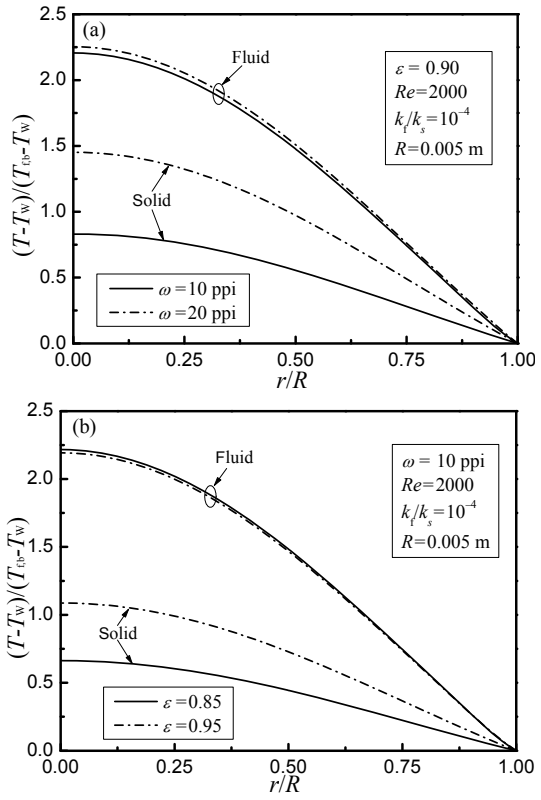

Figure 7 Effect of foam morphology parameters on the temperature profiles in porous foam filled tube. (a) Effect of pore density; (b) effect of porosity.

5.3.3 Comparisons of UWT and UHF

Figure 8 shows the comparison of temperature profiles between UWT of the present semi-analytical solution and UHF of the analytical solution in ref. [14], the same assumptions in the two kinds of boundary conditions are employed. The temperature difference between solid and fluid for UHF is generally more uniform than that of UWT, in particular, the thinner thermal boundary layer is gained for UHF. This result implies that the UHF offers improved heat transfer rate than UWT, and this trend is similar for the smooth tube.

5.4 Heat transfer characteristics

5.4.1 Effects of interia term, axial conduction and thermal dispersion

Figures 9(a) and (b), respectively, show the variations of the Nusselt number with thermal conductivity ratio of $k_{\mathrm{f}}/k_{\mathrm{s}}$ and the Reynolds number under different solving models. The addition of the axial conduction, inertia term, and thermal dispersion can amplify the Nusselt number by comparing the case 1 vs. case 2, case 2 vs. case 3, and case 3 vs. case 4 successively. This result implies that each of the above terms is in favor of the heat transfer in the foam-filled tube.

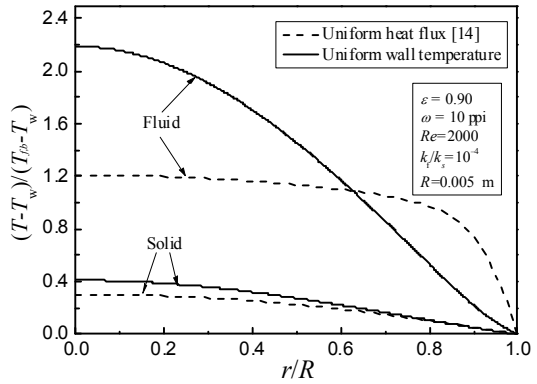

Figure 8 Comparison of the temperature profiles between UWT and UHF.

The value of k_f/k_s varies by changing k_s under fixed k_f, as shown in Figure 9(a). The axial conduction has a significant effect on the Nusselt number in the low thermal conductivity ratio region ($k_f/k_s<4\times10^{-5}$) by comparing cases 1 and 2. This result implies that the portion of axial conduction through solid in the total heat transfer is apparent when the solid thermal conductivity is much higher than that of the fluid. Meanwhile, in the high thermal conductivity ratio region ($k_f/k_s>3\times10^{-3}$), the comparison of cases 3 and 4 shows that the predicted Nusselt number from the numerical solution with thermal dispersion is much higher than without thermal dispersion, revealing that the effect of fluid thermal dispersion is significant when the thermal conductivity of fluid and solid is approaching. Moreover, the comparison of cases 2 and 3 shows that the inertia term has less significant effect on the Nusselt number than the pressure drops (in Figure 5). This can be explained that the heat transfer is both influenced by flow characteristic and heat convection. The inertia term is a nonlinear correction about pressure drop caused by form drag and the flow separation. The interfacial convective heat transfer is a conjugated process which depends on convection term (eq. (5)) and heat conduction of metal framework (eq. (4)). The high heat conductivity of metal framework in comparison to the fluid (such as air or water) leads that the heat conduction of metal framework plays an important role in the overall heat transfer. This induces that the inertia term just has a relatively limited effect on the heat transfer in metal-foam. The similar phenomena had also been found in the study about porous medium conducted by Lage [38]. The contrasting of cases 1 and 4 shows that the predicted Nu of the semi-analytical solution has a deviation of less than 15% from the numerical solution with full model in the range of $4\times10^{-5}<k_f/k_s<3\times10^{-3}$, which covers the thermal conductivity ratio for most of metal to air.

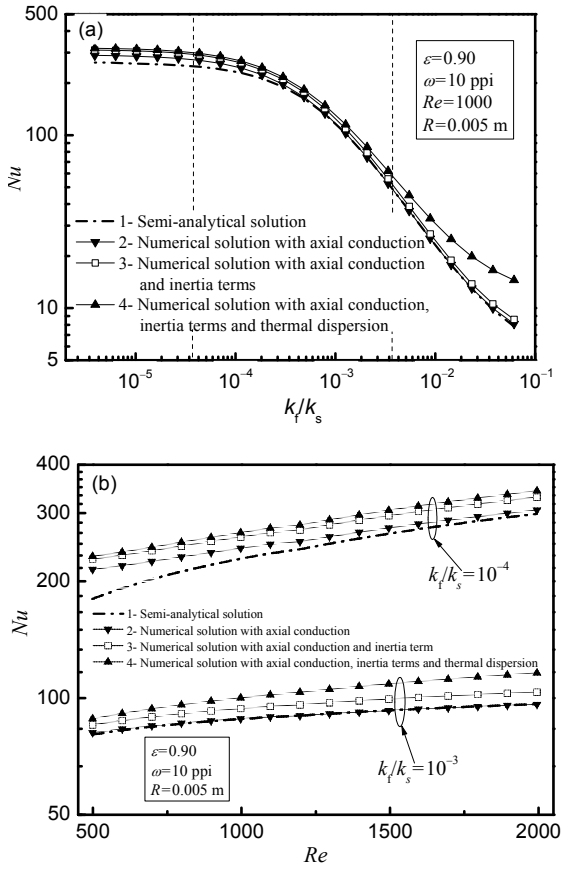

Figure 9 Comparison of the Nusselt number for different solving models. (a) Variation of Nusselt number with thermal conductivity ratio k_f/k_s; (b) variation of Nusselt number with Reynolds number.

As shown in Figure 9(b), the effect of axial conduction on the Nusselt number gradually diminishes as the Reynolds number increases because the contribution of axial conduction to the heat transfer in porous foam becomes smaller when the convective heat transfer becomes stronger by comparing cases 1 and 2. The comparisons of case 2 vs. case 3 and case 3 vs. case 4 present that the effects of inertia term and thermal dispersion moderately amplify with increasing Reynolds number, which is attributed to the fact that the inertia force and the thermal dispersion coefficients are larger for the case with higher flow velocity. In the studied Reynolds number range of $500<Re<2000$, the Nu deviations between the semi-analytical solution and the numerical solution with full model are mostly in the range of 8% to 15%.

5.4.2 *Comparisons of UWT and UHF*

Based on the semi-analytical solution, Figures 10(a) and 10(b) present the comparisons of Nusselt number between the UWT and UHF conditions. The trends of Nu variations with the variation of the corresponding parameters are similar for UWT and UHF; however, the Nusselt number under UWT condition is about 7% to 25% lower than that under UHF condition. As the reference [35], the Nusselt number for smooth tube in the fully developed region under UWT and UHF is 3.65 and 4.36, respectively, and the former is 19.1% lower than the latter.

Figure 10(a) displays the effect of thermal conductivity ratio k_f/k_s on the Nusselt number under UWT and UHF at two fixed Reynolds numbers of 500 and 2000. The Nusselt number increases with the decrease of the k_f/k_s because of the enhancement of solid heat conduction, and the Nusselt number of Re=2000 is naturally higher than Re=500 due to the stronger interfacial heat convection. Moreover, the Nu difference between UHF and UWT is almost unchanged when k_f/k_s varies, indicating that heat conduction has similar contribution on heat transfer enhancement both for UHF and for UWT. However, the Nu deviation for the two kinds of boundary conditions at Re=2000 is larger than at Re=500, indicating that interfacial heat convection has more significant contribution for

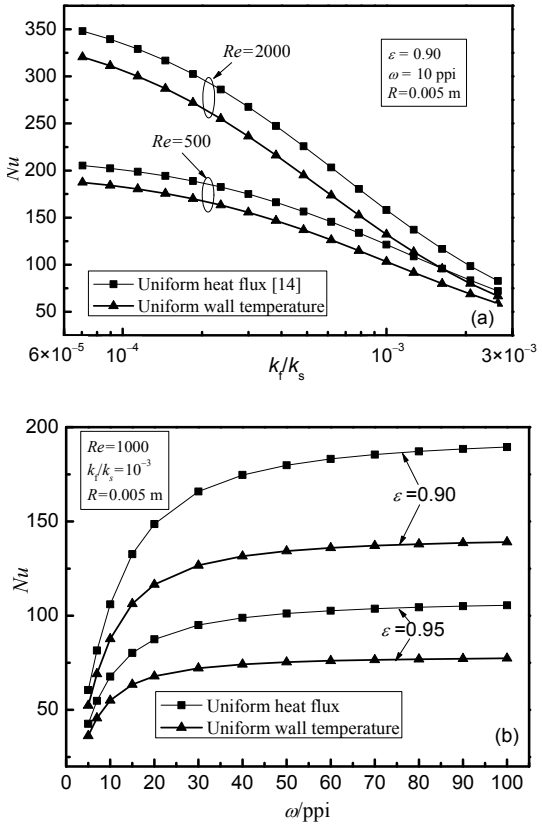

Figure 10 Comparison of Nusselt number between UWT and UHF conditions. (a) Effect of thermal conductivity ratio at two fixed Reynolds number of 500 and 2000; (b) Effect of pore density at two fixed porosity of 0.90 and 0.95.

the case of UHF than that of UWT.

Figure 10(b) shows the variations of the Nusselt number with pore density under the UWT and the UHF at two fixed porosities of 0.9 and 0.95. As the pore density increases, the Nusselt number for both UWT and UHF first increases sharply, and then gradually flattens to a plateau. This result may be due to the fact that the increase of pore density enlarges the interfacial surface, resulting in enhanced convective heat transfer. Furthermore, the Nu difference between UWT and UHF conditions increases gradually with increasing of pore density. This can be explained that the increase of pore density results in the enhancement of interfacial convection and the improvement is more significant for UHF condition than UWT condition. This result is in accordance with the effect of Reynolds number on the Nu difference, as presented in Figure 10(a). In addition, the Nu difference of case with ε=0.9 is larger than that with ε=0.95. The decrease of porosity leads to enlarge the interfacial area and the effective thermal conductivity, resulting in the enhanced interfacial convection and solid conduction. As also indicated in Figure 10(a), the Nu difference between UHF and UWT is nearly unchanged when the portion of heat conduction is enhanced. Hence, it can be speculated that the increment of Nu difference with decreasing porosity is ascribed to the enhancement of heat convection rather than that of solid conduction. Therefore in other words, it can be indicated from the Figures 10(a) and (b) that the heat transfer performance difference between UHT and UWT in porous medium is mainly determined by interfacial convection rather than solid conduction.

6 Conclusions

The fully developed forced convection in a metal-foam filled tube under UWT condition is semi-analytically solved based on the Brinkman-Darcy model and the simplified two-equation model. The predicted results are compared with results from the two-dimensional numerical simulation with full governing equations. The thermal entrance length of the metal foams is shorter than that of the smooth tube. The semi-analytical solution is verified by temperature profile predicted from the numerical solution with identical assumptions. The inertia term has a significant role for the prediction of velocity profile and pressure drop; however, it has a relatively limited impact on the Nusselt number. The axial conduction in the energy equations has obvious effects on the Nusselt number for the case with low Reynolds number or low thermal conductivity ratio ($k_f/k_s<4\times10^{-5}$), and the effects of thermal dispersion can be neglected when the thermal conductivity ratio between the fluid and the solid is remarkably smaller for metallic foam, as example ($k_f/k_s<3\times10^{-3}$). The predicted Nusselt number of the semi-analytical solution is about 8% to 15% lower than that of the numerical solution with full model when $4\times10^{-5}<k_f/k_s<3\times10^{-3}$ as the ratio for typical metal to air. The fluid temperature gradient under UWT is lower than that under UHF, and the temperature profile of solid for UWT is more sensitive to porous morphology parameters than that of fluid. The predicted Nusselt number of UWT is about 7% to 25% lower than that of UHF in the present study range. The heat transfer difference between UWT and UHF is mainly determined by interfacial convection rather than solid conduction.

This work was supported by the National Natural Science Foundation of China (Grant No. 51176149), and the National Basic Research Program of China ("973" Project) (Grant No. 2011CB610306).

1 Chen Z S, Xie W H, Hu P, et al. An effective thermodynamic transformation analysis method for actual irreversible cycle. Sci China Tech Sci, 2013, 56: 2188–2193
2 Lu Y W, Li X L, Li Q, et al. Numerical simulation and experimental investigation of natural convection heat transfer of molten salt around fine wire. Sci China Tech Sci, 2013, 56: 1651–1656
3 Xia G D, Zhai Y L, Cui Z Z. Characteristics of entropy generation and heat transfer in a microchannel with fan-shaped reentrant cavities and internal ribs. Sci China Tech Sci, 2013, 56: 1629–1635
4 Lee D Y, Vafai K. Analytical characterization and conceptual assessment of solid and fluid temperature differentials in porous media.

Int J Heat Mass Transfer, 1999, 42: 423–435
5 Vafai K, Tien C L. Boundary and inertia effects on flow and heat transfer in porous media. Int J Heat Mass Transfer, 1981, 24: 195–203
6 Hooman K. A perturbation solution for forced convection in a porous-saturated duct. J Comput Appl Math, 2008, 211: 57–66
7 Zhao B Q, Pantokratoras A, Fang T G, et al. Flow of a weakly conducting fluid in a channel filled with a Darcy–Brinkman–Forchheimer porous medium. Transport Porous Med, 2010, 85: 131–142
8 Dukhan N. Analysis of brinkman-extended darcy flow in porous media and experimental verification using metal foam. J Fluid Eng, 2012, 134: 071201.1–071201.6
9 Hooman K, Merrikh A A. Analytical solution of forced convection in a duct of rectangular cross section saturated by a porous medium. J Heat Transfer, 2006, 128: 596–600
10 Chikh S, Boumedien A, Bouhadef K. Analytical solution of non-Darcian forced convection in an annular duct partially filled with a porous medium. Int J Heat Mass Transfer, 1995, 38: 1543–1551
11 Zhu X D, Zhang J Z, Tan X M. Numerical simulation on heat transfer inside rotating porous disk subjected to local heat flux. Sci China Tech Sci, 2013, 56: 1657–1666
12 Yang C, Nakayama A, Liu W. Heat transfer performance assessment for forced convection in a tube partially filled with a porous medium. Int J Therm Sci, 2012, 54: 98–108
13 Calmidi V V, Mahajan R L. Forced convection in high porosity metallic foam. J Heat Trans, 2000, 122: 557–565
14 Lu W, Zhao C Y, Tassou S A. Thermal analysis on metal-foam filled heat exchangers. Part I: Metal-foam filled tube. Int J Heat Mass Transfer, 2006, 49: 2751–2761
15 Zhao C Y, Lu W, Tassou S A. Thermal analysis on metal-foam filled heat exchangers. Part II: Tube heat exchangers. Int J Heat Mass Transfer, 2006, 49: 2762–2770
16 Xu H J, Qu Z G, Tao W Q. Analytical solution of forced convective heat transfer in tube partially filled with metallic foam using the two-equation model. Int J Heat Mass Transfer, 2011, 54: 3846–3855
17 Qu Z G, Xu H J, Tao W Q. Fully developed forced convective heat transfer in an annulus partially filled with metallic foam: An analytical solution. Int J Heat Mass Transfer, 2012, 55: 7508–7519
18 Chen C C, Huang P C, Hwang H Y. Enhanced forced convective cooling of heat sources by metal-foam porous layers. Int J Heat Mass Transfer, 2013, 58: 356–373
19 Xu H J, Qu Z G, Tao W Q. Thermal transport analysis in parallel-plate channel filled with open-celled metallic foams. Int J Heat Mass Transfer, 2011, 38: 868–873
20 Xu H J, Qu Z G, Lu T J, et al. Thermal modeling of forced convection in a parallel-plate channel partially filled with metallic foams. J Heat Transfer, 2011, 133: 092603-1-9
21 Du Y P, Qu Z G, Zhao C Y, et al. Numerical study of conjugated heat transfer in metal foam filled double-pipe. Int J Heat Mass Transfer, 2010, 53: 4899–4907
22 Kamiuto K, Saitoh S. Fully developed forced-convection heat transfer in cylindrical packed beds with constant wall temperatures. JSME Int J B-Fluids T, 1994, 37: 554–559
23 Hooman K, Haji-Sheikh A, Nield D A. Thermally developing Brinkman–Brinkman forced convection in rectangular ducts with isothermal walls. Int J Heat Mass Transfer, 2007, 50: 3521–3533
24 Nield D A, Kuznetsov A V, Xiong M. Thermally developing forced convection in a porous medium: parallel plate channel with walls at uniform temperature, with axial conduction and viscous dissipation effects. Int J Heat Mass Transfer, 2003, 46: 643–651
25 Nield D A, Kuznetsov A V, Xiong M. Effect of local thermal non-equilibrium on thermally developing forced convection in a porous medium. Int J Heat Mass Transfer, 2002, 45: 4949–4955
26 Kim S Y, Paek J W, Kang B H. Flow and heat transfer correlations for porous fin in a plate-fin heat exchanger. J Heat Transfer, 2000, 122: 572–578
27 Bejan A, Kraus A D. Heat Transfer Handbook. New Jersey: John Wiley & Sons, 2003
28 Sebben S, RABI B. Some extensions of tridiagonal and pentadiagonal matrix algorithms. Numer Heat Tr B-Fund, 1995, 28: 323–357
29 Du L F, Zhang R, Zhang L M. Phase-field simulation of dendritic growth in a forced liquid metal flow coupling with boundary heat flux. Sci China Tech Sci, 2013, 56: 2586–2593
30 Gao Z X, Jiang C W, Lee C H. Improvement and application of wall function boundary condition for high-speed compressible flows. Sci China Tech Sci, 2013, 56: 2501–2515
31 Feng H J, Chen L G, Xie Z H, et al. Thermal insulation constructal optimization for steel rolling reheating furnace wall based on entransy dissipation extremum principle. Sci China Tech Sci, 2012, 55: 3322–3333
32 Tao W Q, Qu Z G, He Y L. A novel segregated algorithm for incompressible fluid flow and heat transfer problems-CLEAR (Coupled and Linked Equations Algorithm Revised) part I: Mathematical formulation and solution procedure. Numer Heat Tr B-Fund, 2004, 45: 1–17
33 Li Z Y, Tao W Q. A new stability-guaranteed second-order difference scheme. Numer Heat Tr B-Fund, 2002, 42: 349–365
34 Nield D A, Bejan A. Convection in Porous Media. 3rd ed. New York: Springer, 2006
35 Lienhard IV J H, Lienhard V J H. A Heat Transfer Textbook. 3rd ed. Massachusetts: Phlogiston Press, 2005
36 Wang L B, Li X X, Lin Z M, et al. Additional description of laminar heat convection in tube with uniform wall temperature. J Thermophys Heat Tr, 2009, 23: 200–205
37 Wang L B, Zhang Q, Li X X. The role of velocity gradient in laminar convective heat transfer through a tube with uniform wall heat flux. Eur J Phys, 2009, 30: 823–833
38 Lage J L. Effect of the convective inertia term on Bénard convection in a porous medium. Numer Heat Tr, 1992, 22: 469–485
39 Calmidi V V. Transport phenomena in high porosity fibrous metal foams. Dissertation of Doctoral Degree. Colorado: University of Colorado, 1998
40 Dai Z, Nawaz K, Park Y G, et al. Correcting and extending the Boomsma–Poulikakos effective thermal conductivity model for three-dimensional, fluid-saturated metal foam. Int Commun Heat Mass, 2010, 37: 575–580

Attached Table. Correlations of the parameters used in study

Parameter	Correlation	Reference
Permeability K	$K = 0.00073\left(1-\varepsilon\right)^{-0.224}\left(d_{\mathrm{f}}/d_{\mathrm{p}}\right)^{-1.11} d_{\mathrm{p}}^{2}$	[14]
Inertia coefficient C_{I}	$C_{\mathrm{I}} = 0.00212\left(1-\varepsilon\right)^{-0.132}\left(d_{\mathrm{f}}/d_{\mathrm{p}}\right)^{-1.63}$	[39]
Specific surface area a_{sf}	$a_{\mathrm{sf}} = \dfrac{3\pi d_{\mathrm{f}}\left[1-\mathrm{e}^{-((1-\varepsilon)/0.04)}\right]}{\left(0.59d_{\mathrm{p}}\right)^{2}}$	[14]

Parameter	Correlation	Reference
Interfacial heat-transfer coefficient h_{sf}	$h_{sf}=\begin{cases}0.76Re_d^{0.4}Pr^{0.37}k_f/d_f, & (1\leqslant Re_d\leqslant 40)\\ 0.52Re_d^{0.5}Pr^{0.37}k_f/d_f, & (40\leqslant Re_d\leqslant 10^3)\\ 0.26Re_d^{0.6}Pr^{0.37}k_f/d_f, & (10^3\leqslant Re_d\leqslant 2\times10^5)\end{cases}$	[14]
Thermal dispersion coefficient k_d	$k_d=C_D(Re_KPr_e)\dfrac{u}{u_m}$, $C_D=0.06$	[13]
Effective thermal conductivities k_e	$k_e=\dfrac{1}{\sqrt{2}(R_A+R_B+R_C+R_D)}$ $R_A=\dfrac{4\lambda}{(2e^2+\pi\lambda(1-e))k_s+(4-2e^2-\pi\lambda(1-e))k_f}$ $R_B=\dfrac{e-2\lambda}{e^2k_s+(2-e^2)k_f}$ $R_C=\dfrac{2(\sqrt{2}-2e)}{\sqrt{2}\pi\lambda^2k_s+2(2-\sqrt{2}\pi\lambda^2)k_f}$ $R_D=\dfrac{2e}{e^2k_s+(4-e^2)k_f}$ $\lambda=\sqrt{\dfrac{\sqrt{2}(2-(3\sqrt{2}/4)e^3-2\varepsilon)}{\pi(3-2\sqrt{2}e-e)}}$, $e=0.198$	[40]

Appendix. Modified Bessel equation

The generic form of modified Bessel equation is $z^2\dfrac{\partial^2 y}{\partial z^2}+z\dfrac{\partial y}{\partial z}-(z^2+\nu^2)y=0$, when $\nu=0$, this equation may be used for solving eq. (17), and the solution is in the form of $y=C_1I_0(z)+C_2K_0(z)$. The coefficients C_1 and C_2 may be obtained by introducing the definite condition of eqs. (20) and (21). The terms $I_0(z)$ and $K_0(z)$ are the zero-order terms of the first and second type modified Bessel function, respectively, which have the following expressions:

$$I_0(z)=\sum_{k=0}^{\infty}\left[\frac{1}{(k!)^2}\left(\frac{z}{2}\right)^{2k}\right],$$

$$K_0(z)=-I_0(z)\ln\left(\frac{z}{2}\right)+\sum_{k=0}^{\infty}\left[\psi(k+1)\frac{1}{(k!)^2}\left(\frac{z}{2}\right)^{2k}\right].$$

The first order of the two types Bessel functions are also applied and shown as follows:

$$I_1(z)=\sum_{k=0}^{\infty}\left[\frac{1}{k!(k+1)!}\left(\frac{z}{2}\right)^{2k+1}\right],$$

$$K_1(z)=I_1(z)\ln\left(\frac{z}{2}\right)+\frac{1}{z}-\frac{1}{2}\sum_{k=0}^{\infty}\left[(\psi(k+1)+\psi(k+2))\frac{1}{k!(k+1)!}\left(\frac{z}{2}\right)^{2k+1}\right].$$

The above four-type functions ($I_0(z)$, $K_0(z)$, $I_1(z)$, $K_1(z)$) may be ascertained by introducing the relations:

$$\psi(z)=\frac{\mathrm{d}}{\mathrm{d}z}\ln\Gamma(z)=-\gamma+\sum_{n=0}^{\infty}\left(\frac{1}{n+1}-\frac{1}{z+n}\right),\quad \gamma=\lim_{n\to\infty}\left(\sum_{m=1}^{n}m-\log n\right).$$

Correlations exist between the first order and second order functions as follows:

$$I_1(z)=I_0'(z),\quad K_1(z)=-K_0'(z),\quad \frac{\mathrm{d}(zI_1(z))}{\mathrm{d}z}=zI_0(z),\quad \frac{\mathrm{d}(zK_1(z))}{\mathrm{d}z}=-zK_0(z).$$